



# A Parametric Study on the Effect of Drainage on Sand Liquefaction under High Overburden Pressure

Waleed El-Sekelly, Ph.D., P.E.<sup>1</sup>; Ricardo Dobry, Ph.D., M.ASCE<sup>2</sup>; and Tarek Abdoun, Ph.D., M.ASCE<sup>3</sup>

**Abstract:** The effect of high overburden pressure above 1 atm on sand liquefaction potential is typically evaluated based on cyclic undrained testing, with the overburden pressure correction factor,  $K_{\sigma} < 1.0$  and  $K_{\sigma}$  decreasing as the pressure increases. Recent centrifuge experiments of a prototype 5 m-thick clean sand layer having a permeability  $1.2 \times 10^{-4}$  m/s, with free drainage at the top and subjected to 1 and 6 atm overburden pressures, show that a high overburden pressure may increase partial drainage. As a result, the measured field overburden pressure factor,  $(K_{\sigma})_{\text{field}}$  was estimated to be >1.0 instead of <1.0 in these centrifuge tests. A parametric study is presented here that extends the centrifuge results for a relative density,  $D_r = 45\%$  and free top drainage, utilizing a high-fidelity, calibrated numerical model (P2Ps and in FLAC 3D). A stepped acceleration base input is used that ensures a uniform cyclic shear stress amplitude at the elevation of maximum pore pressure ratio. The main parameters varied in the numerical study are overburden pressure,  $\sigma'_{v0}$  (1-12 atm); sand permeability, k (10<sup>-6</sup> to 10<sup>-3</sup> m/s); and sand layer thickness, H (2-10 m). A new drainage factor,  $K_{\rm dr} \ge 1.0$ , is proposed to separate the usual undrained  $K_{\sigma}$  from the effect of partial drainage. The recommendation is to evaluate the overburden pressure factor to be used in liquefaction charts,  $(K_{\sigma})_{\text{field}}$ , as the product of two factors,  $(K_{\sigma})_{\text{field}} = K_{\sigma} \times K_{\text{dr}}$ . The study shows that for constant  $\sigma'_{v0} = 6$  atm,  $K_{\text{dr}} \approx 1.4$ –1.7 when  $k = 10^{-4}$  to  $10^{-5}$  m/s, even for a very thick sand layer of H = 10 m. Still for a constant  $\sigma'_{v0} = 6$  atm,  $K_{dr}$  decreases considerably to values close to 1.0 for a low  $k \approx 10^{-5}$  m/s, when the layer thickness is H = 7 or 8m or greater. And for constant  $k \approx 10^{-4}$  m/s and  $\sigma'_{v0} = 12$  atm,  $K_{dr} \approx 1.4$  if H=5-10 m, increasing to  $K_{\rm dr}\approx 1.8$  if the layer thickness decreases to H=2 m. The parametric study provides insight on when the current State-of-Practice of using only undrained  $K_{\sigma}$  becomes too conservative and should be supplemented with consideration of partial drainage through use of factor  $K_{\rm dr}$ . Ready-to-use charts are provided to evaluate  $K_{\rm dr}$  and  $(K_{\sigma})_{\rm field}$  for a  $D_{\rm r}=45\%$  sand layer with free top drainage. DOI: 10.1061/JGGEFK.GTENG-12205. © 2023 American Society of Civil Engineers.

**Practical Applications:** This research challenges conventional notions of sand liquefaction risk assessment. Traditionally, higher overburden pressures were thought to increase this risk, as indicated by the factor  $K_{\sigma} < 1.0$ . However, recent findings, supported by centrifuge experiments and advanced numerical modeling, reveal a more nuanced reality. Under specific field conditions, especially with elevated overburden pressures, partial drainage in clean sand deposits can enhance the layer stability, resulting in  $(K_{\sigma})_{\text{field}}$  values greater than 1.0. This means that high overburden pressures may not necessarily lead to increased liquefaction vulnerability, contrary to previous assumptions. To better guide practical applications, a novel drainage factor,  $K_{\text{dr}}$ , is introduced. When combined with  $K_{\sigma}$ , it provides a more accurate assessment of liquefaction potential. For engineers and practitioners, this means considering both  $K_{\sigma}$  and  $K_{\text{dr}}$  when evaluating the liquefaction potential of loose sand layers with at least one drainage boundary. This study supplies valuable insights into when the current practice of relying solely on undrained  $K_{\sigma} < 1.0$  may be overly conservative. It offers ready-to-use charts to assess  $K_{\text{dr}}$  and  $(K_{\sigma})_{\text{field}}$ , empowering practitioners to make more informed decisions regarding liquefaction risk. It must be noted that an actual field case history is expected to require some engineering judgment due to soil stratigraphy and the usual spatial variability associated with field deposits.

#### Introduction

The effects of earthquake induced liquefaction may cause damage to many types of structures, including dams and embankments.

Note. This manuscript was submitted on August 9, 2023; approved on October 11, 2023; published online on December 30, 2023. Discussion period open until May 30, 2024; separate discussions must be submitted for individual papers. This paper is part of the *Journal of Geotechnical and Geoenvironmental Engineering*, © ASCE, ISSN 1090-0241.

Engineers typically use the simplified procedure proposed by Seed and Idriss (1971) to assess the liquefaction potential of cohesionless deposits. In the simplified procedure, the *site resistance* to liquefaction is represented by the Cyclic Resistance Ratio, CRR. The CRR is obtained from field measurements using the standard penetration test (SPT) or cone penetration test (CPT); or from field measurements of the shear wave velocity ( $V_s$ ). The CRR is used in conjunction with liquefaction triggering charts developed from earthquake case histories for this purpose. The *earthquake demand at the site* is typically represented by the cyclic stress ratio (CSR), estimated using either of the two definitions contained in Eq. (1) as follows:

$$CSR = \tau_{c}/\sigma'_{v0} = 0.65(a_{\text{max}}/g)(\sigma_{v0}/\sigma'_{v0})r_{d}$$
 (1)

where  $a_{\rm max}$  = maximum horizontal ground surface acceleration; g = gravitational acceleration;  $\sigma'_{\rm v0}$  = vertical effective overburden pressure;  $\sigma_{\rm v0}$  = vertical total overburden pressure; and  $\rm r_d$  = stress

© ASCE 04023144-1 J. Geotech. Geoenviron. Eng.

<sup>&</sup>lt;sup>1</sup>Associate Professor, Dept. of Structural Engineering, Mansoura Univ., Mansoura, Egypt; Research Scientist, Division of Engineering, New York Univ. Abu Dhabi, P.O. Box 129188, Abu Dhabi, United Arab Emirates (corresponding author). ORCID: https://orcid.org/0000-0002-6600-646X. Email: welsekelly@mans.edu.eg

<sup>&</sup>lt;sup>2</sup>Emeritus Professor, Dept. of Civil and Environmental Engineering, Rensselaer Polytechnic Institute, 110 8th St., JEC 4049, Troy, NY 12180. Email: dobryr@rpi.edu

<sup>&</sup>lt;sup>3</sup>Global Distinguished Professor, New York Univ. Abu Dhabi, P.O. Box 129188. Abu Dhabi, United Arab Emirates, Email: ta64@nyu.edu

reduction factor. While the basic definition is  $CSR = \tau_c/\sigma'_{v0}$ , with  $\tau_c$  measured directly in the laboratory in undrained cyclic triaxial or direct simple shear tests, the approximation  $\tau_c = 0.65(a_{max}/g)\sigma_{v0}r_d$  is often used in engineering projects. The CSR, defined typically through the use of  $a_{max}$  in Eq. (1), has also been used in the case histories as part of liquefaction chart development. If CSR > CRR in a project, liquefaction is expected to occur and vice versa.

The simplified procedure and its associated liquefaction triggering charts were developed based on case histories from relatively shallow sites (less than 20 m), with an effective overburden of less than 2 atm. As a result, it is considered a reliable tool for liquefaction assessment in most cases. However, in certain projects such as tall earth embankment dams, the foundation soil that is susceptible to liquefaction may experience much higher effective overburden of up to 10 atm or even higher, as noted by Gillette (2013). To address this issue, Seed (1983) proposed conducting undrained cyclic stress-controlled triaxial or simple shear tests at both 1 atm and at the high  $\sigma'_{v0} > 1$  atm, in order to generate a correction factor  $K_{\sigma}$  for that high pressure, as follows:

$$K_{\sigma} = (CRR)_{\sigma_{\sigma,0}'} / (CRR)_1 \tag{2}$$

where  $(CRR)_1$  and  $(CRR)_{\sigma'_{v0}}$  are the cyclic resistance ratios measured in the laboratory at 1 atm and at the overburden pressure of interest,  $\sigma'_{v0}$ , respectively. In these undrained laboratory tests used in Eq. (2), CRR is the CSR needed to trigger liquefaction in a specified number of cycles, N; with  $CSR = \tau_c/\sigma'_{v0}$  for cyclic simple shear tests, and a similar but slightly different definition of CSR and CRR for cyclic triaxial tests. Several different failure criteria are used to define liquefaction triggering, including reaching an excess pore pressure ratio,  $r_u = u/\sigma'_{v0} = 1.0$  in the case of cyclic simple shear tests (u = excess pore water pressure).

The  $K_{\sigma}$  value from Eq. (2) is then applied to the project by generating from the actual CSR of the project a modified cyclic stress ratio =  $\text{CSR}/K_{\sigma}$ , and using this modified CSR to enter the lique-faction chart. The  $K_{\sigma}$  value is invariably less than 1.0 from cyclic undrained tests when the overburden pressure is higher than 1 atm. Thus, an increased CSR—reflecting an increased demand and increased possibility of liquefaction—is utilized in the liquefaction chart in projects involving high overburden pressures.

To avoid performing cyclic undrained tests at both low and high pressures in a given project, engineers often rely on published  $K_{\sigma}$  curves based on those undrained cyclic tests. The current State of Practice (SoP) is based on the two sets of curves shown in Fig. 1, proposed by Youd and Idriss (2001) and Idriss and Boulanger (2008) for relative densities between 40% and 80%. The curves in Fig. 1 are based on a number of publications focused on undrained cyclic test results, including Seed and Harder (1990), Vaid and Thomas (1995), Hynes et al. (1999), Youd and Idriss (2001), Boulanger (2003), Boulanger and Idriss (2004), Idriss and Boulanger (2006, 2008), Montgomery et al. (2012), and Dobry and Abdoun (2015). In addition to the curves using relative density shown in Fig. 1, Idriss and Boulanger (2008) also generated  $K_{\sigma}$  charts based on CPT tip resistance, which generally follow the same decreasing trend of  $K_{\sigma}$  with confining pressure and are widely used in practice.

Two observations on the sets of curves in Fig. 1 are relevant to the current discussion. The first is that they are based on undrained testing, and the second is that they exhibit significant variation in the range of values they provide. For example,  $K_{\sigma}$  ranges between 0.5 and 0.85 at  $\sigma'_{v0} = 6$  atm. The National Research Council of the National Academies (2017) recommended more research to understand the effect of overburden pressure -among other effects- on sand liquefaction behavior in the field.

Ni et al. (2020) and Abdoun et al. (2020) conducted a series of centrifuge experiments where drainage was possible during shaking, and analyzed the resulting data by evaluating  $K_{\sigma}$  under these simulated field conditions, referred to here as  $(K_{\sigma})_{\text{field}}$  to differentiate it from the undrained laboratory  $K_{\sigma}$ . They also conducted regular undrained, stress-controlled cyclic triaxial tests to obtain the conventional laboratory undrained  $K_{\sigma}$ . In each centrifuge test, a clean Ottawa F65 sand layer, 5 m-thick in prototype, with  $D_{\rm r}$  of either 45% or 80% and subjected to  $\sigma'_{\rm v0}=1$  atm and  $\sigma'_{\rm v0}=6$  atm was shaken with 1D base earthquake motions to produce high excess pore pressure ratios. The  $(K_{\sigma})_{\text{field}}$  was found to be greater than 1.0 at  $\sigma'_{v0} = 6$  atm for both loose and dense sand, while the laboratory undrained  $K_{\sigma}$  was 0.85 < 1.0 for  $D_{\rm r} = 45\%$ , consistent with the current state of practice reflected in Fig. 1. The difference between  $(K_{\sigma})_{\text{field}} > 1$  and laboratory undrained  $K_{\sigma} < 1$  was attributed to the partially drained behavior of the sand layer under the idealized field conditions of the centrifuge tests. Partial drainage resulted in a CRR increasing more at 6 atm than 1 atm, due to the lower sand compressibility at 6 atm. Abdoun et al. (2020) suggested further research and parametric studies based on experimental and numerical simulations, in order to better understand this behavior. The significance of such research is that a higher  $K_{\sigma}$  due to partial drainage could potentially reduce unnecessary liquefaction mitigation measures in some situations for tall embankment dams.

Based on the authors' experience gained from their previous experimental and analytical work in Ni et al. (2020) and Abdoun et al. (2020), a numerical parametric study is proposed herein, where the values of  $(K_\sigma)_{\text{field}}$  are obtained for a wide range of possible field scenarios not covered by the original centrifuge experiments.

The main parameters investigated herein are: (a) vertical effective overburden pressure;  $\sigma'_{v0}$ ; (b) sand layer permeability, k; and (c) sand layer thickness, H. The study was conducted using the commercial numerical platform FLAC3D, along with its in-house constitutive model P2Psand.

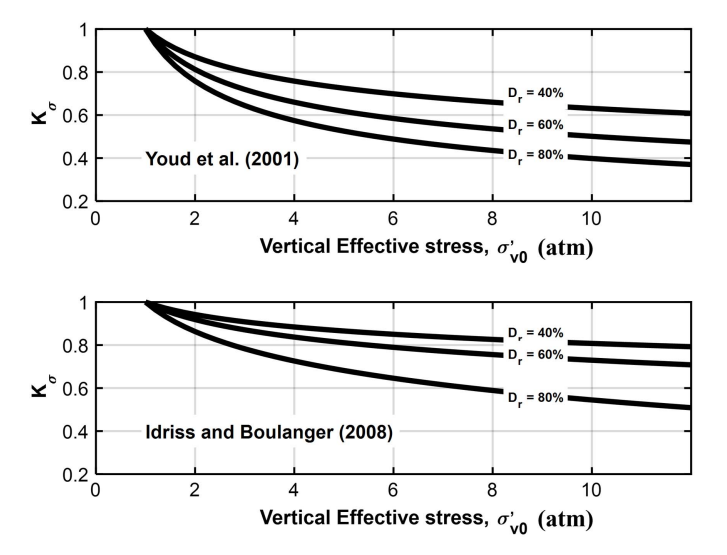


**Fig. 1.**  $K_{\sigma}$  curves for different relative densities proposed by Youd and Idriss (2001) and Idriss and Boulanger (2008). (Reprinted from *Engineering Geology*, Vol. 312, W. El-Sekelly, R. Dobry, and T. Abdoun, "Assessment of state-of-practice use of field liquefaction charts at low and high overburden using centrifuge experiments," 106952, © 2023a, with permission from Elsevier.)

**Table 1.** Relative density, confining pressure and g-level of centrifuge models and FLAC3D simulations

Experiment	Effective overburden pressure, $\sigma'_{v0}$ (atm) <sup>a</sup>	Relative density, $D_{\rm r}$ (%)	Measured experimental pore pressure ratio $r_u = u/\sigma'_{v0}$		Numerical FLAC3D simulation Actual recorded acceleration	FLAC3D simulation Stepped acceleration
			Top (minimum)	Bottom (maximum)	input-El-Sekelly et al. (2022)	input-El-Sekelly et al. (2023a, b)
Test 45-1	1	45	0.42	0.80	FLAC 45-1	FLAC 45-1 ST
Test 45-6	6	45	0.13	0.76	FLAC 45-6	FLAC 45-6 ST
Test 80-1	1	80	0.44	0.92	_	_
Test 80-6	6	80	0.14	0.60	_	_

<sup>&</sup>lt;sup>a</sup>Effective overburden pressure before shaking at mid depth of sand layer.

### Significance of Partial Drainage Revealed by the Centrifuge Experiments

The studies conducted by Ni et al. (2020) and Abdoun et al. (2020) involved four centrifuge model experiments, identified as Tests 45-1, 45-6, 80-1, and 80-6 in Table 1. These tests were labeled based on the relative density  $(D_r)$  and the average vertical effective overburden pressure  $(\sigma'_{v0})$  applied at the center of the liquefiable layer at the specified centrifuge g-level  $(D_{\rm r} - \sigma'_{\rm v0})$ . As presented in Table 1, the tests covered a broad range of  $D_{\rm r}$  (45 and 80%) and  $\sigma'_{v0}$  (1 and 6 atm or ~100 and 600 kPa). The parametric study presented herein focuses on  $D_{\rm r} = 45\%$ , which is more critical to liquefaction evaluation. The experiments were performed in a lightweight laminar container made of aluminum, mounted on a shaking table placed on the platform of Rensselaer Polytechnic Institute's centrifuge machine. The simulations replicated a saturated sand layer around 5 meters thick in prototype using Ottawa F65 sand, a soil commonly employed in research projects such as LEAP (El Ghoraiby et al. 2017; Manzari et al. 2018). The model sand layer had an impervious base and a free drainage boundary at the top, allowing for free drainage through the superimposed strata, as illustrated in Fig. 2.

The centrifuge models consisted of a prototype 5 m-thick layer of dry pluviated, saturated Ottawa F65 sand, with a thin transition filter layer of coarse sand on top, overlain by a layer of lead shot

that varied in thickness depending on the experiment. The purpose of the lead shot layer was twofold: (1) to provide the necessary static weight needed to reach the desired overburden; and (2) to provide the mass and corresponding lateral inertia and horizontal shear stresses acting on the sand during shaking. The sand was saturated with a viscous fluid of appropriate viscosity depending on the centrifuge g-level, to ensure that the same fluid flow behavior was reproduced in the experiments in all cases corresponding to the same water flow behavior at 1g. The models underwent 10 uniform, approximately sinusoidal horizontal base motions with a prototype frequency of 2 Hz, generating significant excess pore water pressure buildup (u), close to, but not quite reaching initial liquefaction, defined by a maximum excess pore pressure ratio in the layer,  $(r_{\rm u})_{\rm max} = (u/\sigma'_{\rm v0})_{\rm max} = 1.0$ . The actual measured  $(r_{\rm u})_{\rm max}$  values ranged from 0.60 to 0.92, as listed in Table 1. For more information on the tests and interpreted results, see Ni et al. (2020) and Abdoun et al. (2020).

Fig. 3 shows the time histories of input acceleration, as well as the measured histories of shear stress ratio (shear stress  $(\tau)/\sigma'_{v0}$ ) and excess pore pressure ratio  $(r_{\rm u})$  near the bottom of the sand layer—where the maximum  $r_{\rm u}=(r_{\rm u})_{\rm max}$  was observed—all recorded during shaking in Tests 45-1 and 45-6. The acceleration and pore pressure histories in Fig. 3 were directly measured with the corresponding sensors, and the shear stresses were evaluated from the measured accelerations in the sand using system identification

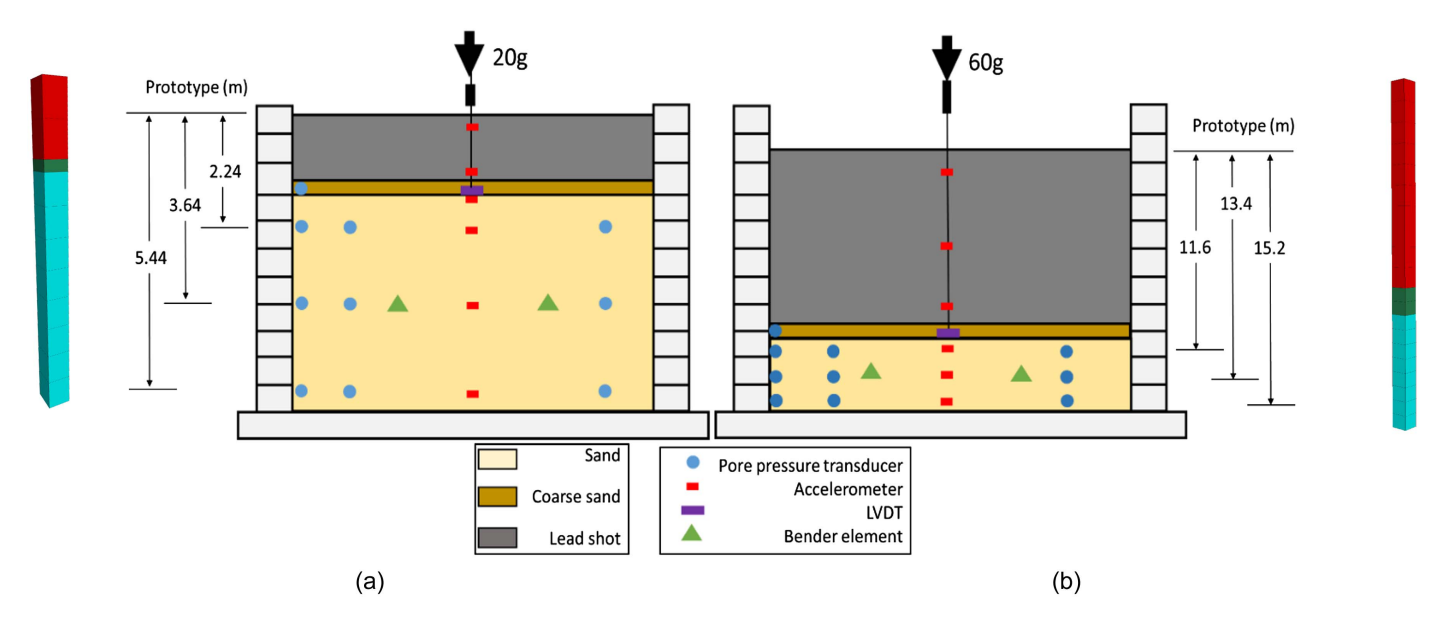


**Fig. 2.** Physical and numerical model layout for: (a) low confining pressure centrifuge experiment (Test 45-1), and (b) high confining pressure centrifuge experiment (Test 45-6). (Adapted from Ni et al. 2020; El-Sekelly et al. 2022.)

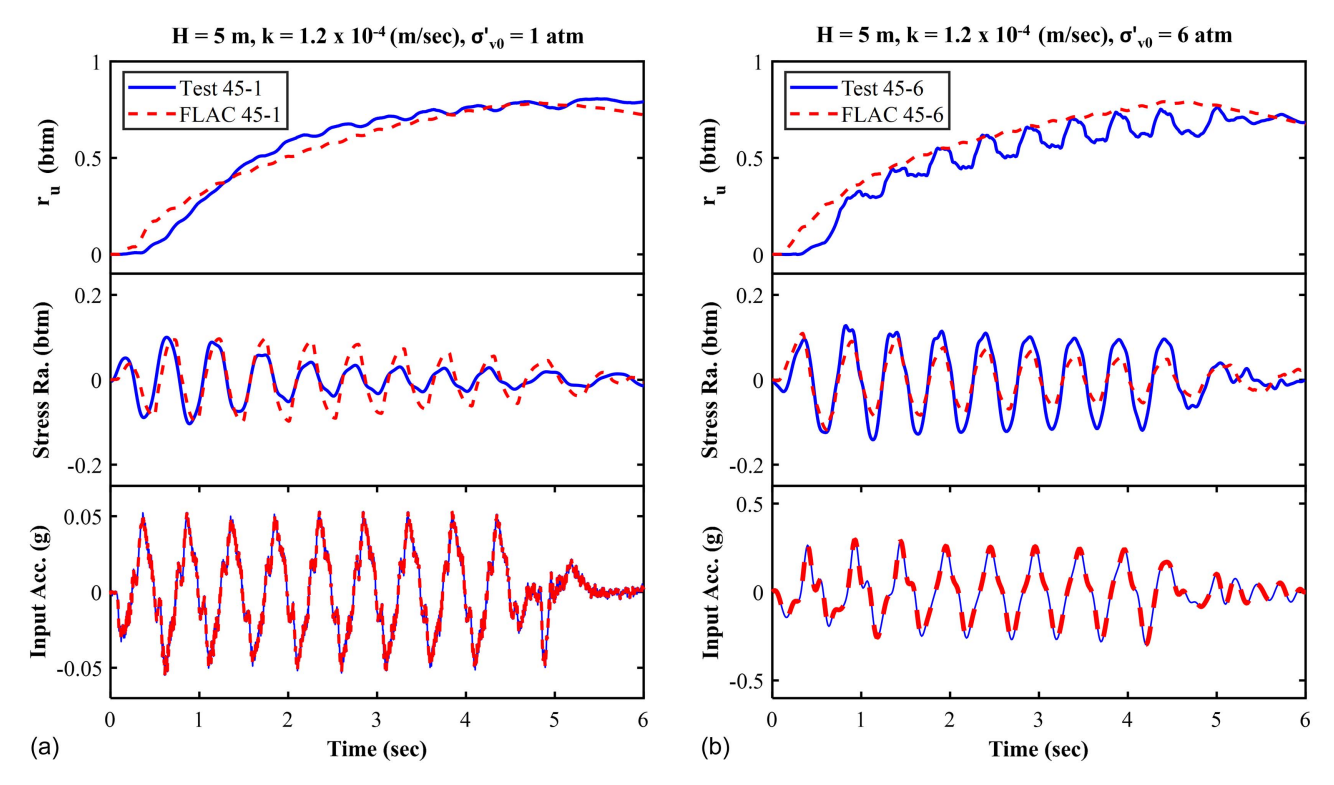


**Fig. 3.** Experimentally recorded and numerically computed histories of excess pore pressure ratio, shear stress ratio, and input acceleration at the bottom of the sand layer, for (a) Test 45-1 and simulation FLAC 45-1; and (b) Test 45-6 and simulation FLAC 45-6.

(Elgamal et al. 1995; Zeghal et al. 1995). The figure also shows the time history plots obtained by El-Sekelly et al. (2022) from the Flac3D numerical simulations discussed in the following section.

Only the key results are shown in Fig. 3 and Table 1 for brevity, with the full results reported elsewhere (refer to Ni et al. (2020) for full experimental results). The test results presented by Ni et al. show that: (a) The maximum excess pore pressure ratio,  $(r_u)_{max}$ , was consistently located near the bottom of the sand layer, close to the impervious boundary; (b) the excess pore pressure ratio,  $r_u$ , was at a minimum near the top of the sand layer, close to the pervious boundary, clearly indicating that partial drainage took place in the upper part of the layer; and (c) the partial drainage was more prominent at 6 atm than at 1 atm, as concluded from the lower values of  $r_u$  at shallower elevations and higher hydraulic gradients observed in the 6 atm tests compared to the 1 atm tests.

Ni et al. (2020) obtained a value for  $(K_{\sigma})_{\text{field}} = 1.28$  using Eq. (2) from the centrifuge experiments at  $D_{\rm r}=45\%$  (Tests 45-1 and 45-6 in Table 1). The calculation was based on a failure criterion of  $(r_u)_{max} = 0.8$  after 10 shaking cycles, as this was indeed the  $(r_{\rm u})_{\rm max}$  measured at the end of shaking in these two centrifuge experiments (Table 1 and Fig. 3). The two values of CRR used in Eq. (2) were the representative median  $\tau_c$  and corresponding CSR in the sand associated with the first few cycles of shaking, before stress-strain degradation started due to the pore pressure buildup. The rationale was that the simplified procedure uses values of  $\tau_c$ and CSR that assume no pore pressure buildup and no stress-strain degradation (Youd and Idriss 2001). This  $(K_{\sigma})_{\text{field}} = 1.28$  obtained from centrifuge Tests 45-1 and 45-6 for  $\sigma'_{\rm v0}=6$  atm is greater than 1.0, and much higher than the range of  $K_{\sigma} = 0.50$ –0.85 provided by the SoP curves in Fig. 1. As already discussed herein, these SoP values are based on cyclic undrained laboratory tests, while the centrifuge experiments were partially drained rather than undrained. Abdoun et al. (2020) attributed the higher intensity of drainage during shaking in the centrifuge at 6 atm (with the corresponding decrease in excess pore pressures and increase in shear stresses and CSR at 6 atm needed to reach the  $(r_{\rm u})_{\rm max}=0.80$ ), to the increased constrained modulus, M', and coefficient of consolidation,  $c_{\rm v}$ , of the sand layer at 6 atm. This was supported by a detailed analysis of the centrifuge measurements, showing that M' and  $c_{\rm v}$  were 2–3 times higher at 6 atm than at 1 atm. This factor of 2–3 is approximately equal to the square root of the ratio of overburden pressures ( $\sqrt{(6/1)}=\sqrt{6}=2.4$ ); the commonly accepted rule for expressing the change in sand volumetric stiffness with effective confining pressure.

# Numerical Simulations Using FLAC3D (El-Sekelly et al. 2022)

El-Sekelly et al. (2022) conducted numerical simulations of centrifuge Tests 45-1 and 45-6 of sand at  $D_r = 45\%$ , using FLAC3D and the P2Psand model. P2Psand was calibrated with triaxial experiments and then refined with the centrifuge results. Additional detail about the P2Psand model calibration procedure is provided by El-Sekelly et al. (2022). The numerical simulations were performed in prototype scale and their aim was to replicate a soil column in the center of the centrifuge model far from the boundaries. The numerical model was composed of 8-nodes brick zones stacked on top of each other, and connected at the nodes in order to simulate a shear beam response of the centrifuge laminar container. Initially, geostatic conditions were established using the Mohr-Coulomb soil model, with the base fixed and sides allowed to move only vertically. Then, the dynamic phase of the analysis was initiated with the P2Psand model assigned to the sand and the sides allowed to move freely. The simulations reproduced the hydraulic boundary conditions of the centrifuge tests, with impervious sides and base and a pervious top layer. The numerical exercise was a fully coupled effective stress simulation, taking into account pore pressure generation, dissipation, and redistribution. Additional details can be found in El-Sekelly et al. (2022).

Figs. 3(a and b) illustrate the results of these simulations, Flac 45-1 and Flac 45-6, of centrifuge Tests 45-1 and 45-6, and compare them to the measured data. Both simulations used the corresponding base input accelerations actually recorded in the centrifuge tests. The shear stress ratio records in both simulations show remarkable agreement with the experiments, particularly in the first few cycles, after which the amplitudes started to degrade as the excess pore pressure increased. Moreover, Figs. 3(a and b) demonstrate that the computed excess pore pressure ratio,  $r_u$  closely match the experimental records for both 1 and 6 atm. Due to the very good similarity in the stress ratio between numerical and experimental simulations in the first few cycles of shaking, the numerically computed  $(K_\sigma)_{\text{field}} = 1.29$  was also essentially identical to  $(K_\sigma)_{\text{field}} = 1.28$  obtained experimentally by Ni et al. (2020), using the same calculation method.

It must be noted that the same square root rule for the dependency of sand stiffness on effective confining pressure, previously mentioned and observed in the centrifuge experiments, is incorporated in FLAC3D for both shear modulus, G and bulk modulus, K. These moduli are in turn used to determine the coefficient of diffusivity, G, from Biot (1955), with G being analogous to the coefficient of consolidation G0 in the classical theory of consolidation proposed by Terzaghi et al. (1996) (see also Abdoun et al. 2020 and El-Sekelly et al. 2022 for additional information).

While the use of the actual input acceleration in numerical simulations such as Flac 45-1 and Flac 45-6 by El-Sekelly et al. (2022), provided good agreement with the centrifuge results as shown in Fig. 3, it is not well suited to the parametric study of  $(K_{\sigma})_{\text{field}}$  which is the focus of this paper. The reason is the difficulty in defining for each run, the shear stress,  $\tau_c$ , and corresponding stress ratio,  $CRR = CSR = \tau_c/\sigma'_{v0}$  at the elevation of interest, needed for the computation of  $(K_{\sigma})_{\text{field}}$  with Eq. (2). This difficulty was not present in simulations Flac 45-1 and Flac 45-6 just discussed, where undegraded values of  $\tau_{\rm c}$  and CSR could be identified in both runs shown in Fig. 3 at the beginning of shaking. However, determining  $\tau_c$  and CSR proved to be much more challenging in other parametric numerical runs attempted by the authors, where significant pore pressure buildup and corresponding stress-strain degradation started early in the shaking and no clear value of  $\tau_{\rm c}$  could be obtained. Therefore, it was decided to switch in the parametric study to the stepped input acceleration approach recently introduced by El-Sekelly et al. (2023b) and discussed under the next heading.

### FLAC3D Simulations Using a Stepped Acceleration Input (El-Sekelly et al. 2023b)

It is a common practice for numerical modelers to simulate *undrained* stress-controlled *single element* cyclic direct simple shear (CDSS) tests in numerical platforms such as FLAC3D, using a stepped input velocity. El-Sekelly et al. (2023b) proposed a modified approach for *partially drained* simulations of *soil profiles* containing a sand layer, where a stress-controlled cyclic CDSS-type of loading is achieved at all sand elevations by using a stepped acceleration input, as sketched in Fig. 4 and explained as follows.

The stepped accelerations in FLAC3D simulations sketched in Fig. 4 and used by El-Sekelly et al. (2023b), involved several 8-node brick zones stacked on top of each other, forming a soil column connected at the nodes. Shear beam behavior was achieved by connecting each node to the three other nodes on the same level so

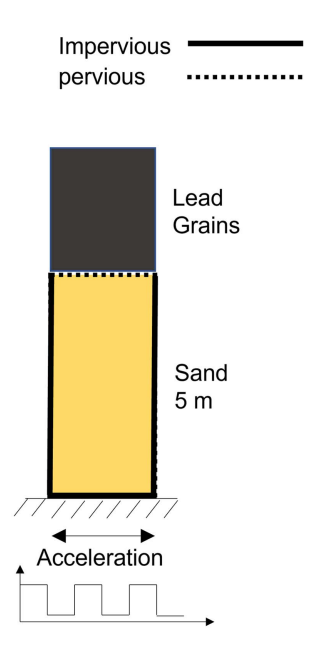


**Fig. 4.** Partially drained sand layer within a soil column simulated numerically using stepped base input acceleration.

that they moved together. The initial geostatic stresses in the soil were established using the Mohr-Coulomb soil model.

In the dynamic phase of the simulation, the soil column was fixed at the base and was free elsewhere, with the sand assigned the P2Psand constitutive model. The sides and bottom of the soil column were impervious, while the top was a free drainage boundary. The fluid was allowed to freely flow between the vertically stacked zones, resulting in a one-dimensional fully coupled mechanical-fluid flow analysis.

A stepped acceleration function was applied at the base (Figs. 4) and 5). The times at which the base acceleration reversed its sign were coded to the software and corresponded to the time at which the shear stress at a specific elevation reaching a maximum positive or negative level predefined before the run,  $\tau_c$ . The specific elevation at which this maximum shear stress condition was enforced corresponded to the elevation of calculated maximum pore pressure ratio within the sand layer,  $r_u = (r_u)_{max}$ , which was iteratively determined by trial and error. For the top free drainage condition, similar to the centrifuge experiment with the same permeability of Ottawa F65 sand, the elevation of this maximum pore pressure ratio was located near the bottom of the sand layer. In those undrained runs where drainage essentially did not occur because of the very low sand permeability, conducted also using the stepped acceleration approach to obtain the undrained  $K_{\sigma} = (K_{\sigma})_{\text{field}}$ , the elevation of maximum pore pressure ratio was near the top of the sand layer. This procedure guaranteed that  $\tau_{\rm c}$  was the same for all cycles at the elevation where  $r_{\rm u}=(r_{\rm u})_{\rm max}$  (Fig. 5), with a tendency for the duration of these cycles to increase with time of shaking as the whole sand layer experienced stress-strain degradation.

### Validation of Stepped Acceleration Method Using Centrifuge Results and Undrained $K_{\sigma}$

In order to validate this stepped acceleration approach, El-Sekelly et al. (2023b) used it to simulate the same two centrifuge experiments discussed earlier (runs Flac 45-1 ST and Flac 45-6 ST listed in Table 1 and plotted in Fig. 5). The amplitude of the acceleration input at the base of the soil column was adjusted to generate shear

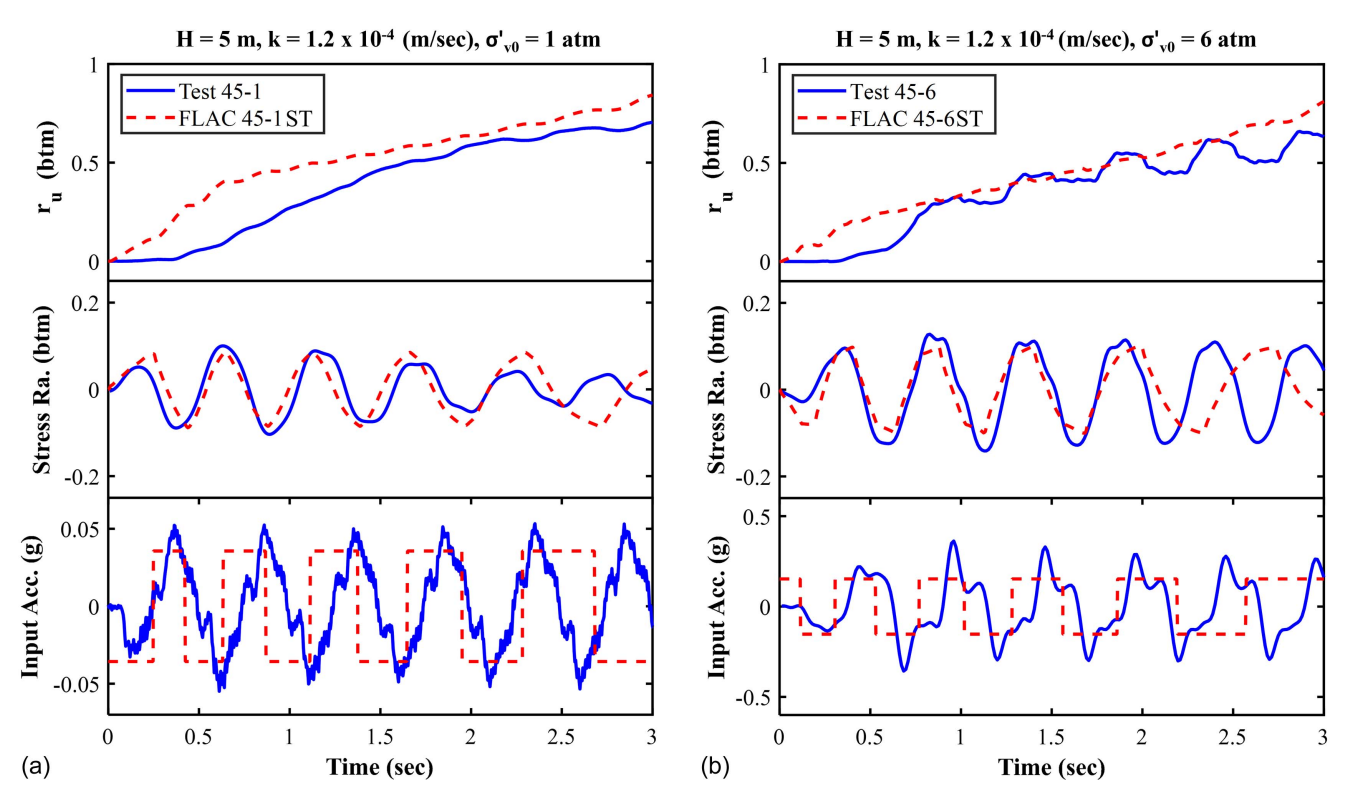


**Fig. 5.** Experimentally recorded and numerically computed time histories of excess pore pressure ratio, shear stress ratio, and input acceleration at the bottom of the sand layer, for (a) Test 45-1 and simulation FLAC 45-1 ST; and (b) Test 45-6 and simulation FLAC 45-6ST (El-Sekelly et al. 2023b).

stress cycles of similar amplitude to those actually measured in the centrifuge experiments near the bottom of the sand layer. Comparisons of the experimental and simulated results in terms of input acceleration, shear stress ratio near the bottom of the sand, as well as the time history of the excess pore pressure ratio, r<sub>u</sub>, at the same elevation, showed good agreement (Fig. 5). However, there was a difference in pore pressure response at the beginning of shaking, mainly because the first cycle of the input acceleration in the experiment was smaller than the rest of the acceleration cycles. El-Sekelly et al. (2023b) also found that  $r_u$  reached a maximum value of 0.8 after only five cycles of shaking in the stepped input numerical simulation, unlike the centrifuge experiment which reached  $r_{\rm u} = 0.8$  after ten loading cycles. On the contrary, most of the generated  $r_{\rm u}$  in the experiments was reached also after the first five cycles of loading, with the rest of the shaking causing a very small increase in  $r_{\rm u}$ . Therefore, El-Sekelly et al. (2023b) decided to limit the duration of the two numerical simulations Flac 45-1 ST and Flac 45-6 ST to the first five cycles, as shown in Fig. 5, with the calculated  $r_{ij}$  being relatively similar to the experimental  $r_{ij}$  at the end of the five cycles. N = 5 cycles was finally adopted by the authors as the standard for the acceleration input in the whole parametric study. The choice of 5 loading cycles correspond to an earthquake of magnitude, M = 6 (Idriss and Boulanger 2008), which has a relatively short duration. This shortened duration within the stepped input acceleration context, has the additional advantage of preventing the input acceleration cycles and shear stress cycles within the sand to become too long in duration, as the sand experiences stress-strain degradation and an increased cycle duration becomes necessary to reach the specified  $\tau_c$  at the elevation of interest.

In order to calculate both the undrained  $K_{\sigma}$  as well as the partially drained  $(K_{\sigma})_{field}$  utilizing this stepped acceleration procedure, the liquefaction strength curves (LSC) were constructed at 1 and

6 atm, as curves of cyclic stress ratio (CSR) versus number of cycles (N) needed to reach  $(r_{\rm u})_{\rm max}=0.80$  in the sand layer. This is the same format generally utilized for laboratory undrained cyclic tests, but now developed from the Flac3D runs that used a stepped acceleration input. This was done for both very low permeability sand (undrained) as well as for the partially drained conditions (top drainage), which simulates the centrifuge situation.

Fig. 6(a) shows the LSCs at 1 and 6 atm for the undrained runs (very low sand permeability) which indicates that the LSC at 6 atm is below that at 1 atm, similar to the predictions of the state of practice for undrained testing. Since this case represents an undrained situation, the ratio  $(CRR)_{6 \text{ atm}}/(CRR)_{1 \text{ atm}}$  is indeed the usual  $K_{\sigma}$ , which is found from the data in Fig. 6(a) to be about 0.8 for N=5 loading cycles. This value is consistent with the current state of practice, which predicts  $K_{\sigma}$  within the range of 0.67 (Youd and Idriss 2001) and 0.84 (Idriss and Boulanger 2008) for this relative density,  $D_{\rm r}=45\%$ , and for the vertical overburden pressure,  $\sigma'_{v0}=6$  atm (Fig. 1).

Fig. 6(b) shows the LSCs at 1 and 6 atm for a soil column with the same permeability of the centrifuge experiments and the same drainage condition of free top drainage and undrained bottom boundary. The two runs for N=5 cycles are the same as Flac 45-1 ST and Flac 45-6 ST, already discussed. The corresponding ratio  $(K_\sigma)_{\rm field} = {\rm CSR}_{\rm 6\,atm}/{\rm CSR}_{\rm 1\,atm}$  was found to be 1.15 at 5 cycles for this partially drained case. This shows the increased effect of partial drainage at the higher overburden pressure (6 atm), as compared to lower overburden pressure (1 atm). The  $(K_\sigma)_{\rm field} = 1.15$  obtained from this method is relatively similar but lower than  $(K_\sigma)_{\rm field} = 1.28-1.29$ - obtained from the centrifuge experiments as well as from numerical simulations Flac -45-1- and Flac -45-6-in Table 1, that used the original sinusoidal input base acceleration. But most importantly, these  $(K_\sigma)_{\rm field}$  values are all clearly above 1.0, unlike the undrained  $K_\sigma$  which is below 1.0.

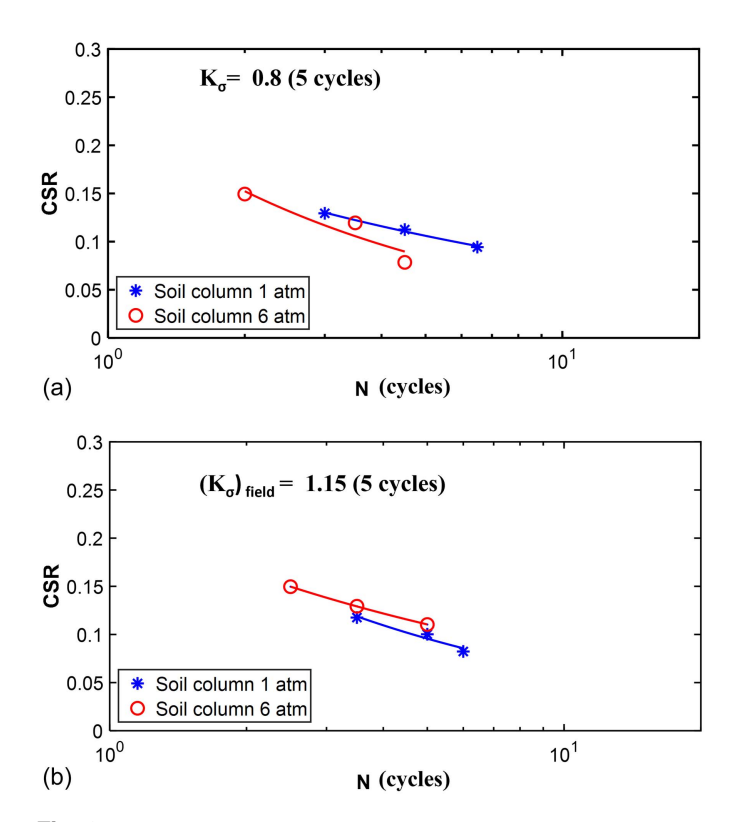


**Fig. 6.** Liquefaction strength curves (LSC) from FLAC3D numerical simulations of soil column using the P2Psand model and stepped acceleration input, of: (a) undrained sand layer; and (b) partially drained sand layer. All data points and curves correspond to the CSR needed to reach  $(r_{\rm u})_{\rm max}=0.80$  in N cycles.  $(K_{\sigma})$  and  $(K_{\sigma})_{\rm field}$  are both defined as  $({\rm CSR})_{\rm 6\,atm}/({\rm CSR})_{\rm 1\,atm}$  for N=5 cycles.

As mentioned before, the failure criteria adopted in this study is defined by reaching  $(r_{\rm u})_{\rm max}=0.8$  after 5 loading cycles. It is important to test the sensitivity of adopting different failure criteria based on  $(r_{\rm u})_{\rm max}$  other than 0.8, or a number of cycles needed to reach  $(r_{\rm u})_{\rm max}$  other than 5 cycles. Fig. 7 provides insight into the influence of different failure criteria on  $(K_{\sigma})_{\rm field}$  and  $K_{\sigma}$ . Figs. 7(a and c) show that  $(K_{\sigma})_{\rm field}$  remains essentially unchanged when different failure criteria, represented by  $(r_{\rm u})_{\rm max}=0.8$  or 0.9, or N=5 or 10 cycles, are adopted, as evidenced by the data points closely aligned along the 45-degree lines in these two graphs. The data

points in Figs. 7(a and c) were obtained from the stepped acceleration FLAC3D runs done in the parametric study and discussed in the next section, and correspond to a range of scenarios. Fig. 7(b) shows analogous results for the undrained cyclic triaxial tests presented by Ni et al. (2020), indicating that the undrained  $K_{\sigma}$  is insensitive to the level of excess pore pressure ratio considered within the range of 0.8-1.

### **Parametric Study**

This section reports the results of the parametric study on  $K_{\sigma}$  and  $(K_{\sigma})_{\rm field}$ , focused on an extension of the centrifuge test results of a sand layer of  $D_{\rm r}=45\%$  having an impervious base and a drainage top boundary. The main factors studied are: (a) effective overburden pressure,  $\sigma'_{\rm v0}$ ; (b) permeability, k; and (c) deposit thickness, H. All runs were conducted using the stepped base acceleration approach, with a failure criterion of  $r_{\rm u}=(r_{\rm u})_{\rm max}=0.80$  after N=5 cycles of shaking. The effect of different parameters and combinations of parameters are discussed under the following subheadings on the basis of the summary Figs. 8–13.

### Effect of Overburden Pressure, $\sigma'_{v0}$ (Figs. 8 and 9)

The effect of the overburden pressure on the undrained  $K_{\sigma}$ , was studied by conducting runs similar to those presented in Fig. 6(a) for the sand layer in an undrained condition [for which  $(K_{\sigma})_{\text{field}}$ becomes equal to  $K_{\sigma}$ , but now extending the  $\sigma'_{v0} = 1$  and 6 atm values used in Fig. 6(a) to a wider range of  $\sigma'_{v0}$  between 1 and 12 atm. The results are presented in Fig. 8 as the red data points and curve of  $K_{\sigma}$  versus  $\sigma'_{v0}$ . The graph also includes the SoP curves recommended by Youd and Idriss (2001) and Idriss and Boulanger (2008) from Fig. 1 for  $D_r = 45\%$ , with both based on undrained test results. The data points from the parametric study in Fig. 8 are generally bounded by the two SoP curves, with a somewhat steeper trend. That is, the FLAC3D data points are closer to the Idriss and Boulanger (2008) curve up to  $\sigma'_{v0}$  of about 8 atm, and then gradually approach the Youd and Idriss (2001) curve for greater  $\sigma'_{v0}$ . This reasonable consistency between  $K_{\sigma}$  computed by FLAC3D and the SoP curves serves as additional validation, and provides a useful cornerstone for the detailed parametric study of  $(K_{\sigma})_{\text{field}}$  presented in the rest of the section.

The effect of overburden pressure on  $(K_{\sigma})_{\text{field}}$  was also studied for the same soil column, but now having the sand permeability and drainage conditions of the centrifuge experiments. The results are

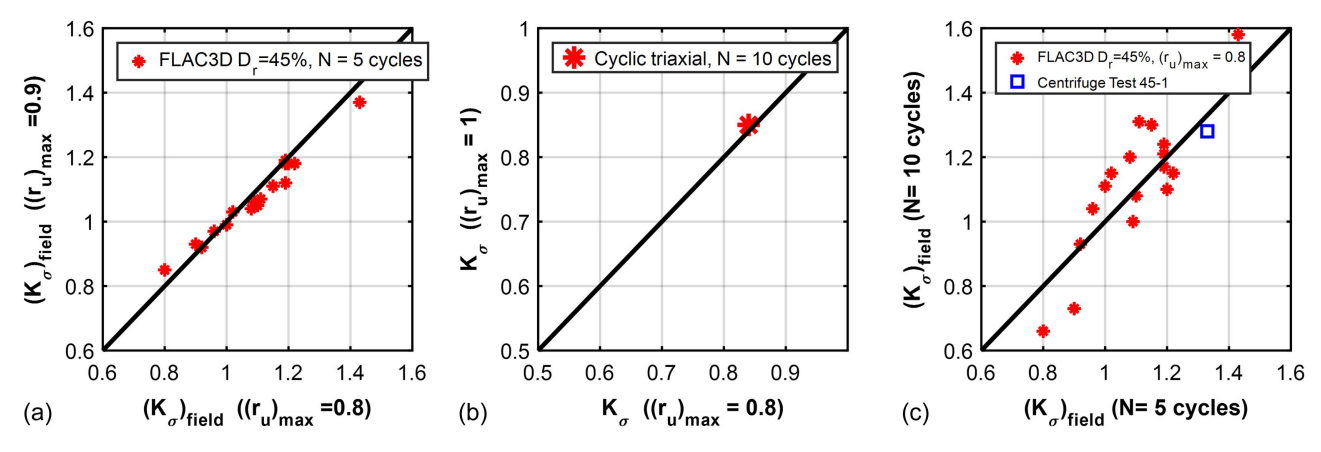
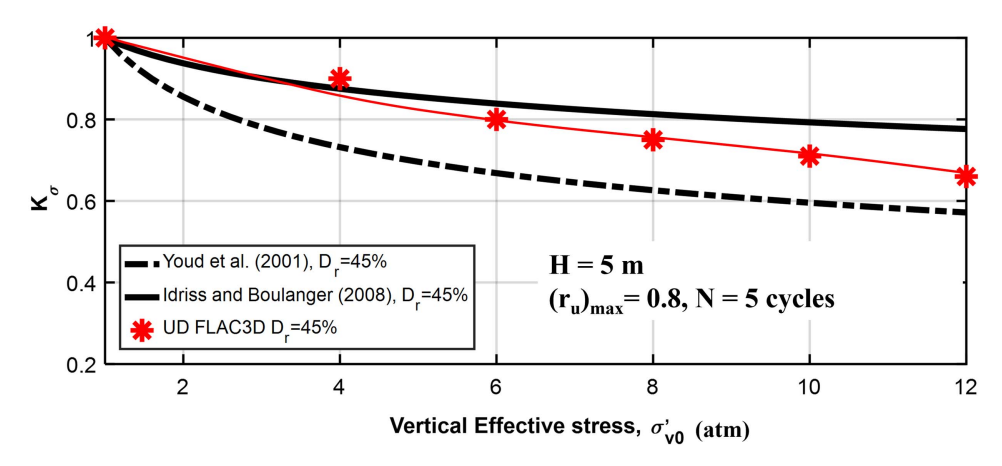


Fig. 7. Influence of selected failure criteria on  $(K_{\sigma})_{\text{field}}$  and  $K_{\sigma}$ , for: (a)  $(K_{\sigma})_{\text{field}}$  using  $(r_{\text{u}})_{\text{max}} = 0.8$  versus 0.9 in FLAC3D simulations; (b)  $K_{\sigma}$  using  $(r_{\text{u}})_{\text{max}} = 0.8$  versus 0.9 in undrained cyclic triaxial tests; and (c)  $(K_{\sigma})_{\text{field}}$  using N = 5 versus 10 cycles in FLAC3D simulations.



**Fig. 8.** Effect of overburden pressure on  $K_{\sigma}$  from undrained soil column FLAC3D simulations of sand at  $D_{\rm r} = 45\%$  (data points and thin curve); and comparison with the SoP curves from Fig. 1 (thick curves).

shown by the data points and curve of Fig. 9(a), which exhibits a mildly curved bell shape with a peak at 6 atm.

There are two ways to interpret this bell-shaped curve in Fig. 9(a). One is to look at Eq. (2), and conclude that while generally  $CRR_{\sigma'_{v_0}} > CRR_{1 \, atm}$  in the range between 1 and 12 atm, the two cyclic stress ratios are about equal,  $CRR_{\sigma'_{v_0}} \approx CRR_{1 \, atm}$  and thus  $(K_{\sigma})_{field} \approx 1$  at the two ends of the range; for pressures about 1 and 12 atm. Moreover, the effect of partial drainage was found to be maximum at

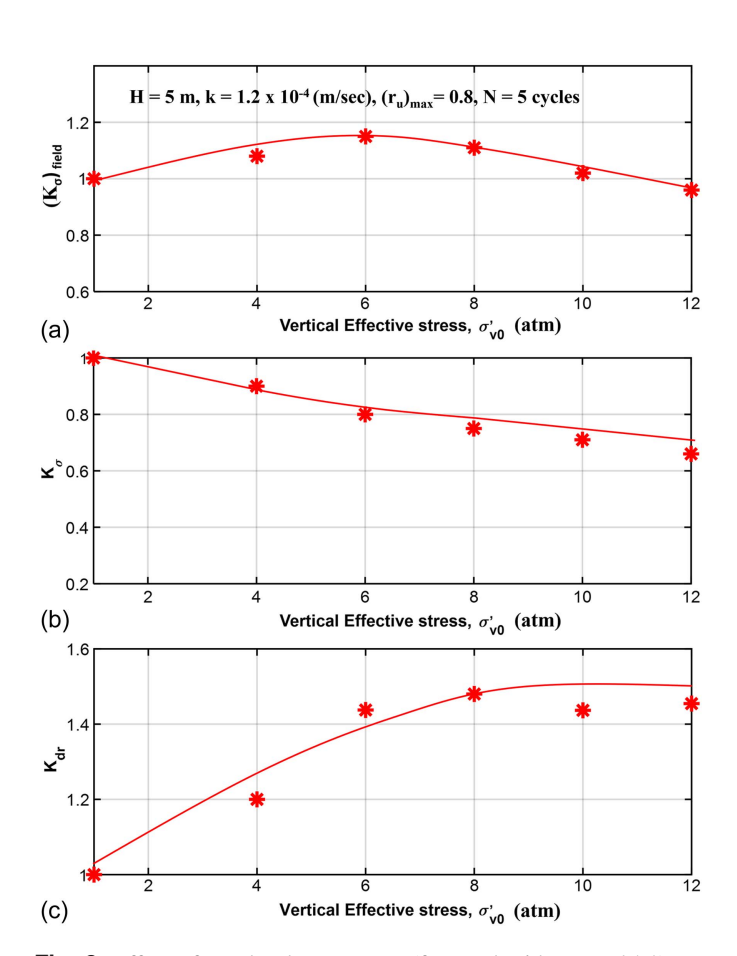


**Fig. 9.** Effect of overburden pressure (for sand with  $D_{\rm r}=45\%$ ) on: (a)  $(K_{\sigma})_{\rm field}$  for partially drained soil column FLAC3D simulations; (b) undrained  $K_{\sigma}$  from Fig. 8 using FLAC3D simulations; and (c)  $K_{\rm dr}=(K_{\sigma})_{\rm field}/K_{\sigma}$  obtained by dividing the curves in (a and b).

about 6 atm. While this is an interesting pattern, there is a second interpretation that the authors feel is more useful in reference to the SoP.

This other way of looking at the curve of Fig. 9(a) is to focus on its possible usage in engineering projects. In current practice, as already discussed in a previous section, in a project involving a large  $\sigma'_{v0} > 1$  atm, the actual  $(\text{CSR})_{\sigma'_{v0}}$  is divided by the undrained  $K_{\sigma}$  before using it to enter the liquefaction chart, in order to obtain the appropriate equivalent  $(\text{CSR})_{1\,\text{atm}}$  consistent with the chart, with  $K_{\sigma} < 1.0$  obtained for example from Figs. 1 or 8. That is,  $(\text{CSR})_{1\,\text{atm}} = (\text{CSR})_{\sigma'_{v0}}/K_{\sigma}$ , consistent with the definition of  $K_{\sigma}$  in Eq. (2), which was based on CRR instead of CSR. This is perfectly fine if liquefaction in the field is expected not to be affected by partial drainage. If partial drainage needs to be considered, the expression should be modified to  $(\text{CSR})_1 = (\text{CSR})_{\sigma'_{v0}}/(K_{\sigma})_{\text{field}}$ , with  $(K_{\sigma})_{\text{field}}$  obtained for example from Fig. 9(a). As it will be typically that  $(K_{\sigma})_{\text{field}} > K_{\sigma}$ , it is useful to define a new proposed drainage factor,  $K_{\text{dr}}$ , such that:

$$(K_{\sigma})_{\text{field}} = K_{\sigma} \times K_{\text{dr}} \tag{3}$$

with  $K_{\rm dr} \geq 1.0$  reflecting exclusively the beneficial effect of partial drainage depending on the actual field conditions. Fig. 9(b) reproduces the same curve of  $K_{\sigma}$  obtained using undrained FLAC3D runs from Fig. 8. Fig. 9(c) includes the corresponding curve for the new coefficient,  $K_{\rm dr} = (K_{\sigma})_{\rm field}/K_{\sigma}$ , obtained by simply dividing the datapoints of Fig. 9(a) by those of Fig. 9(b). As expected, in Fig. 9(c)  $K_{\rm dr} = 1$  at 1 atm, and always greater than 1.0 for larger vertical effective pressures. The value of  $K_{\rm dr}$  increases up to approximately 6 atm, beyond which it levels off at a value of about 1.45. Based on the observed trend, it may be assumed that the trendline will remain relatively flat beyond 12 atm. It must be noted, however, that most practical field applications are expected to be below 12 atm. If needed, it is recommended that this trend be verified by extra numerical simulations above 12 atm.

Therefore, in this proposed interpretation which is useful in practical applications, the user in a given project would first evaluate the undrained  $K_{\sigma}$  the usual way [e.g., from Figs. 1 or 9(b)], then would evaluate the value of  $K_{\rm dr}$  for the actual loading and drainage conditions of the project [e.g., from Fig. 9(c)], finally obtaining the  $(K_{\sigma})_{\rm field}$  using Eq. (3), and then calculating the desired  $({\rm CSR})_1 = ({\rm CSR})\sigma'_{v0}/(K_{\sigma})_{\rm field}$  needed to enter the liquefaction chart.

 $K_{
m dr}$  is mostly used throughout the rest of this parametric study as a more useful way to present the results than  $(K_\sigma)_{
m field}$ . It is understood that once  $K_{
m dr}$  is known, the original value of  $(K_\sigma)_{
m field}$ 

calculated in the parametric study can always be retrieved using Eq. (3) and  $K_{\sigma}$  from Figs. 8 or 9(b).

### Effect of Permeability, k (Fig. 10)

This part of the parametric study investigates the effect of the permeability on  $(K_\sigma)_{\rm field}$  and  $K_{\rm dr}$ . Fig. 10(a) shows that  $(K_\sigma)_{\rm field}$  increases with permeability, with  $(K_\sigma)_{\rm field}$  being about equal to the (undrained)  $K_\sigma=0.8$  for the lowest permeability included in the graph (about  $10^{-6}$  m/s). The figure also shows the datapoints corresponding to  $K_\sigma$  from the SoP curves of Idriss and Boulanger (2008) and Youd and Idriss (2001) in Fig. 1, for  $D_{\rm r}=45\%$  and an overburden pressure of 6 atm. It can be seen that at this low permeability,  $(K_\sigma)_{\rm field}$  is generally consistent with the undrained  $K_\sigma$  from the SoP, as expected. An additional validation in Fig. 10(a)

is provided by the data point for  $(K_\sigma)_{\rm field}$  obtained directly from the centrifuge results as calculated by Ni et al. (2020), plotted at the prototype permeability of the sand in the centrifuge,  $k=1.2\times 10^{-4}$  m/s. Fig. 10(b) is similar to Fig. 10(a) but now in terms of  $K_{\rm dr}$  obtained with Eq 3.

### Combined Effect of Overburden Pressure, $\sigma'_{v0}$ , and Layer Thickness, H (Fig. 11)

The effect of overburden pressure on  $K_{\rm dr}$  was previously shown in Fig. 9(c) for a 5 m thick sand layer of permeability,  $k=1.2\times 10^{-4}$  m/s, similar to the sand layer parameters in the centrifuge. The study in Fig. 9(c) of the effect of overburden on  $K_{\rm dr}$  for H=5 m is extended in Fig. 11 to layers having a thickness, H=2 and 10 m, all with the same permeability  $k=1.2\times 10^{-4}$  m/s.

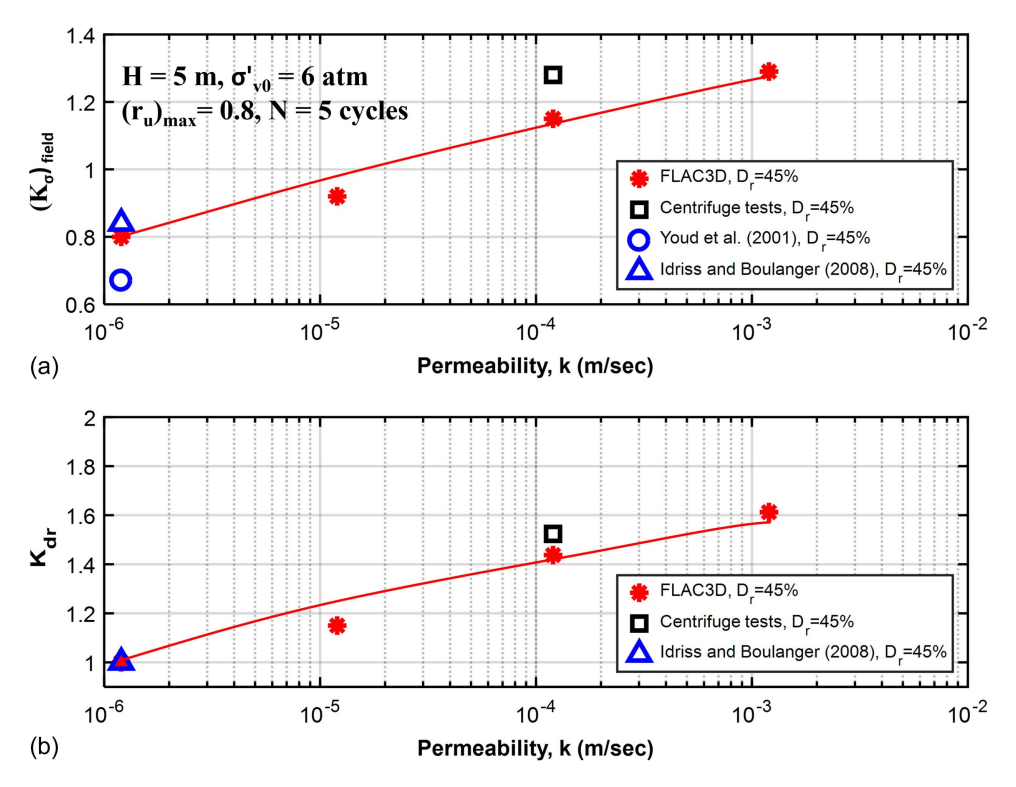


**Fig. 10.** Effect of permeability on: (a)  $(K_{\sigma})_{\text{field}}$ ; and (b)  $K_{\text{dr}}$ , for partially drained soil column FLAC3D simulations of sand with  $D_{\text{r}} = 45\%$ .

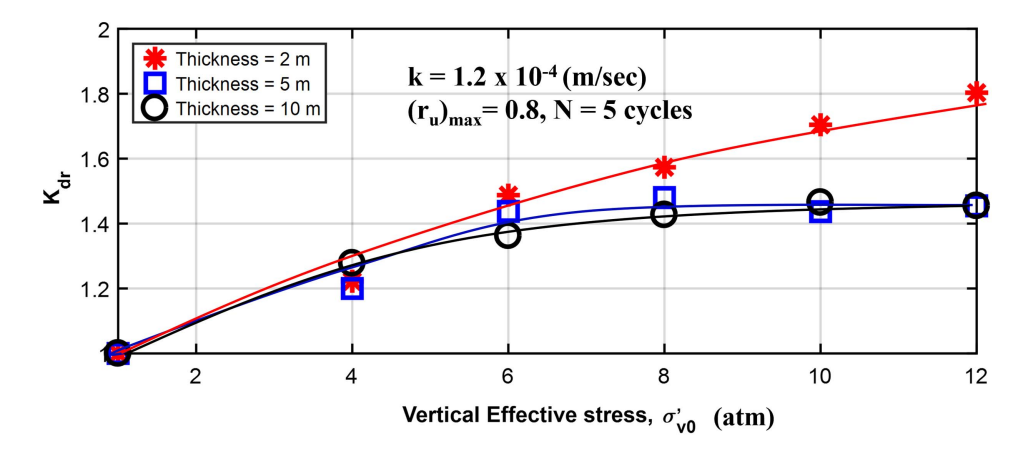


**Fig. 11.** Effect of overburden pressure,  $\sigma'_{v0}$ , on  $K_{dr}$  for partially drained soil column FLAC3D simulations, H = 2, 5 or 10 m thick sand layer with  $D_r = 45\%$ .

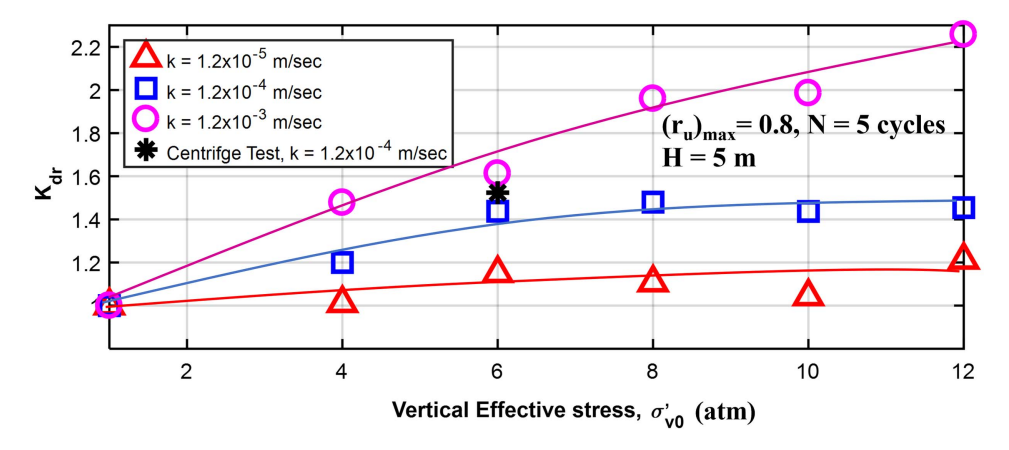


**Fig. 12.** Effect of overburden pressure,  $\sigma'_{v0}$ , on  $K_{dr}$  of partially drained soil column FLAC3D simulations for sand layers having permeabilities,  $k = 1.2 \times 10^{-5}$ ,  $1.2 \times 10^{-4}$ , or  $1.2 \times 10^{-3}$  m/s with  $D_r = 45\%$ .

The results in Fig. 11 demonstrate that for all three thicknesses (2, 5, and 10 m), the trend for  $K_{\rm dr}$  is almost identical up to an overburden pressure of approximately 6 atm. After this point, the curves corresponding to 5 and 10 m define a plateau with a maximum  $K_{\rm dr}$  of approximately 1.45. In contrast, the  $K_{\rm dr}$  of the 2 m thick deposit continues to increase up to  $K_{\rm dr}=1.8$  at the maximum studied overburden pressure of 12 atm. This suggests that the beneficial effect of partial drainage of an upper drainage boundary, is about the same for a layer thickness in the range from 5 to 10 m, becoming much more significant for a thinner (2m-thick) sand layer.

## Combined Effect of Overburden Pressure, $\sigma'_{v0}$ , and Permeability, k (Fig. 12)

Again, the effect of overburden pressure on  $K_{\rm dr}$  was previously shown in Fig. 9(c) for a 5 m thick sand deposit of permeability,  $k=1.2\times 10^{-4}$  m/s, which corresponds to the conditions in the centrifuge experiments. Fig. 12 shows the effect of pressure on  $K_{\rm dr}$  extended to a lower  $k=1.2\times 10^{-5}$  m/s and to a higher  $k=1.2\times 10^{-3}$  m/s, in all cases with H=5 m. The results indicate that the higher the permeability, the higher the value of  $K_{\rm dr}$ , reflecting as expected an increased beneficial effect of the partial drainage.

Specifically, for the low permeability  $(1.2 \times 10^{-5} \text{ m/s})$ ,  $K_{\rm dr}$  remains relatively low in the order of approximately 1.1–1.2 between 4 and 12 atm. At the other extreme, the high permeability runs  $(1.2 \times 10^{-3} \text{ m/s})$  exhibit a steadily increasing  $K_{\rm dr}$  up to a maximum value of about 2.2 at the highest considered overburden pressure of 12 atm. For the intermediate permeability associated with the centrifuge experiments  $(1.2 \times 10^{-4} \text{ m/s})$ ,  $K_{\rm dr}$  grows and reaches a plateau in the order of about 1.45 at an overburden pressure of approximately 6 atm. The figure suggests that the for this case of  $D_{\rm r}=45\%$  and free drainage at the top, the beneficial effect of partial drainage, as reflected in the value of  $K_{\rm dr}$ , is quite sensitive to the permeability of the sand.

# Combined Effect of Layer Thickness, H, and Permeability, k (Fig. 13)

Fig. 13 shows the combined effects of the deposit thickness, H, and permeability, k, on  $K_{\rm dr}$  with the overburden pressure,  $\sigma'_{\rm v0}$ , held constant at 6 atm in the middle of the layer. The results again show that a higher permeability leads to a higher  $K_{\rm dr}$ . Additionally, it can be observed that  $K_{\rm dr}$  decreases only slightly when the layer thickness increases at both intermediate and high permeabilities. Specifically,

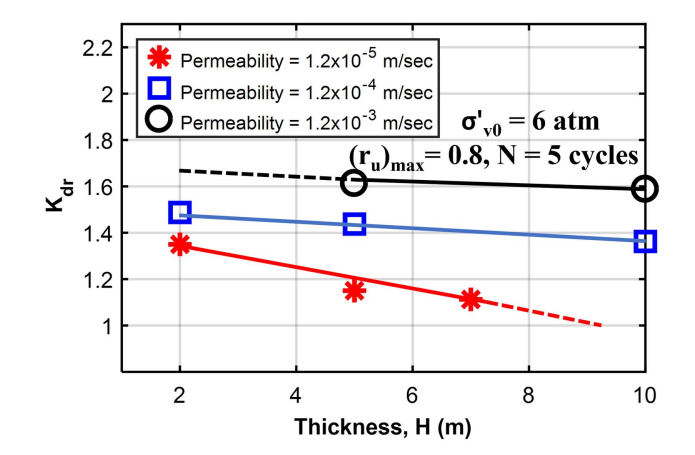


**Fig. 13.** Effect of sand layer thickness on  $K_{\rm dr}$  of partially drained soil column FLAC3D simulations for sand layers having permeabilities,  $k = 1.2 \times 10^{-5}$ ,  $1.2 \times 10^{-4}$ , or  $1.2 \times 10^{-3}$  m/s with  $D_{\rm r} = 45\%$ .

 $K_{\rm dr}$  averages around 1.6 and 1.4 at these high and intermediate permeabilities, respectively. Alternatively, at the low permeability,  $k=1.2\times 10^{-5}$  m/s, the effect of deposit thickness on  $K_{\rm dr}$  is much more pronounced, with  $K_{\rm dr}$  decreasing from about 1.35 for H=2 m to about 1.1 for H=7 m. Overall, the results indicate a tendency for  $K_{\rm dr}$  to decrease as H increases, as expected, but with the decrease being more significant for the low permeability layer.

#### **Summary and Discussion**

Based on centrifuge experiments conducted at 1 and 6 atm, Ni et al. (2020) concluded that liquefaction field response may not be fully undrained in some cases, but rather partially drained, with this partial drainage being more pronounced when the overburden pressure is higher. These tests clearly showed that partial drainage increased sand liquefaction resistance more significantly at 6 atm compared with 1 atm, resulting in a  $(K_\sigma)_{\text{field}} > 1$ , unlike the SoP recommendations of  $K_\sigma < 1$  of Fig. 1. Abdoun et al. (2020) demonstrated that the increased partial drainage at high overburden was due to increased sand constrained modulus M' and coefficient of consolidation  $c_v$ . They recommended additional centrifuge tests, as well as parametric studies of  $(K_\sigma)_{\text{field}}$  based on calibrated numerical simulations, to extend the results of the experiments.

El-Sekelly et al. (2022) used the FLAC3D numerical platform and calibrated the P2Psand model with cyclic triaxial results, refining the calibration with the Ni et al. (2020) centrifuge measurements (Fig. 3). The calibrated parameters of the P2Psand model were independent of confining pressure and hence could be used in a general parametric study. However, such parametric study could not be completed by El-Sekelly et al. (2022) due to the fast pore pressure buildup and fast stress-strain degradation in the sand layer at the beginning of shaking in some of the runs. This fast stress-strain degradation prevented selection of the undegraded CSR = CRR for the run, needed to determine  $(K_{\sigma})_{\text{field}}$  using Eq. (2). Subsequently, El-Sekelly et al. (2023b) proposed a new approach, where the same soil profile with calibrated P2Psand model for the sand layer is subjected to a stepped acceleration base input instead of the sinusoidal input acceleration used in Figs. 3–5.

The parametric study of  $(K_\sigma)_{\rm field}$  presented herein in Figs. 8–13 used such stepped input acceleration, applied to a profile containing a saturated Ottawa sand layer of  $D_{\rm r}=45\%$  which is free to drain at the top, and defining CRR as the CSR needed to reach  $(r_{\rm u})_{\rm max}=0.80$  in N=5 shaking cycles. The main parameters varied in the study were: (a) confining pressure,  $\sigma'_{\rm v0}$  (1 to 12 atm); (b) permeability,  $k~(\approx 10^{-6}~{\rm to}~10^{-3}~{\rm m/s})$ ; and (c) deposit thickness, H (2-10 m). The effect of confining pressure for a very low permeability (and hence undrained) sand layer, was studied first for  $(K_\sigma)_{\rm field}=K_\sigma$ , with the results matching well the SoP undrained  $K_\sigma$  (Fig. 8). This provided added confidence on the validity of the numerical methodology. A new practical drainage factor,  $K_{\rm dr}$ , was proposed to separate the undrained  $K_\sigma$  from the effect of partial drainage, such that  $(K_\sigma)_{\rm field}=K_\sigma\times K_{\rm dr}$  [Eq. (3)].

The results of the parametric study reveal the following:

- Varying  $\sigma'_{v0}$  between 4 and 12 atm while maintaining the same permeability ( $k = 1.2 \times 10^{-4} \text{ m/s}$ ) and deposit thickness (5 m) results in an increase in  $K_{\rm dr}$  up to a point where the trend follows a plateau after  $\sigma'_{v0} = 6$  atm. This maximum  $K_{\rm dr}$  between 6 and 12 atm is around 1.45 (Fig. 9).
- Varying k between  $1.2 \times 10^{-6}$  and  $1.2 \times 10^{-3}$  m/s while maintaining the same  $\sigma'_{v0}$  (6 atm) and layer thickness (5 m) of the centrifuge tests, results in an increasing trend for  $K_{\rm dr}$ , reaching a maximum value of  $K_{\rm dr} \approx 1.6$  at the highest permeability studied (Fig. 10).
- Varying  $\sigma'_{v0}$  between 4 and 12 atm as well as the thickness between 2 and 10 m, while maintaining the same permeability of the centrifuge tests ( $k=1.2\times 10^{-4}$  m/s), results in an increasing trend of  $K_{\rm dr}$  with  $\sigma'_{v0}$ , up to a point where the trend follows a plateau at  $\sigma'_{v0}=6$  atm for both H=5 and 10 m ( $K_{\rm dr}\approx 1.45$ ). For H=2 m, the increasing trend continues until reaching  $K_{\rm dr}\approx 1.8$  at 12 atm (Fig. 11).
- Varying  $\sigma'_{v0}$  between 1 and 12 atm as well as k between  $1.2 \times 10^{-5}$  and  $1.2 \times 10^{-3}$  m/s, while maintaining the same layer thickness (5 m) of the centrifuge tests, reveals that permeability plays a significant role in determining the effect of partial drainage on  $K_{\rm dr}$  and  $((K_\sigma)_{\rm field})$ . When the permeability is relatively low  $(k=1.2\times 10^{-5} {\rm m/s})$ ,  $K_{\rm dr}$  is generally low and below about 1.2, even at a high overburden. When the permeability is high  $(k=1.2\times 10^{-3} {\rm m/s})$ ,  $K_{\rm dr}$  increases rapidly up to about 2.2 at  $\sigma'_{v0}=12$  atm. For the intermediate permeability  $(k=1.2\times 10^{-4} {\rm m/s})$ , corresponding to the situation in the centrifuge tests,  $K_{\rm dr}$  reaches a maximum value of about 1.45 at 6 atm, and more or less maintains this value up to 12 atm (Fig. 12).
- Varying the deposit thickness between H=2 and 10 m and the permeability between  $k=1.2\times 10^{-5}$  and  $1.2\times 10^{-3}$  m/s, while maintaining the same  $\sigma t_{v0}$  (6 atm) of the centrifuge tests, shows that the effect of thickness is not very significant for a range of intermediate to high permeabilities ( $k=1.2\times 10^{-4}$ )

to  $1.2 \times 10^{-3}$  m/s). That is, all values of  $K_{\rm dr}$  are in the range 1.4–1.7 for all combinations of intermediate/high permeability and H=2–10 m. However, for a low permeability (k =  $1.2 \times 10^{-5}$  m/s), there is a clear inverse trend, with  $K_{\rm dr}$  decreasing from about 1.35 down to a value close to 1 when the thickness increases from 2 to 7 m (Fig. 13).

#### **Conclusions**

The conclusions of this research are as follows:

- 1. The effect of a high overburden pressure above 1 atm on sand liquefaction potential, as measured by the factor  $K_{\sigma}$ , has historically been established based on cyclic undrained testing, with  $K_{\sigma} < 1.0$  and  $K_{\sigma}$  decreasing as the overburden increases.
- 2. Recent centrifuge experiments by Ni et al. (2020) of a clean sand layer with impervious base and free top drainage, supplemented by numerical analyses by El-Sekelly et al. (2022, 2023b), suggest that liquefaction response may not always be undrained in the field, with a high overburden pressure increasing partial drainage and hence decreasing liquefaction potential. This is reflected in  $(K_{\sigma})_{\text{field}} > 1.0$  and a tendency for  $(K_{\sigma})_{\text{field}}$  to *increase* as the overburden increases for certain field conditions. Therefore, it is not true that a high overburden will always increases the liquefaction vulnerability in the field, as assumed in the current use of liquefaction charts in conjunction with  $K_{\sigma} < 1.0$ .
- 3. A high-fidelity, calibrated numerical model (P2Psand in FLAC3D) was used to perform a parametric study of the values of  $(K_{\sigma})_{\rm field}$  and of the new proposed practical drainage factor  $K_{\rm dr} = (K_{\sigma})_{\rm field}/K_{\sigma} > 1$ , that extended and generalized the centrifuge results. For a sand layer of  $D_{\rm r} = 45\%$  and free top drainage, the parametric study focused on the effects of overburden pressure (1-12 atm), permeability  $(1.2 \times 10^{-6} \text{ to } 1.2 \times 10^{-3} \text{ m/sec})$ , and layer thickness (2-10 m). The parametric study showed that:
  - for constant  $\sigma'_{v0} = 6$  atm, the value of  $K_{dr}$  is in the narrow range 1.45-1.65 when the sand permeability is in the range  $10^{-4}$  to  $10^{-5}$  m/s, even if the layer thicknesses is increased to 10 m.
  - for constant  $\sigma'_{v0} = 6$  atm,  $K_{dr}$  decreases significantly to values close to, or even lower than 1.0 if the sand permeability is low ( $\approx 10^{-5}$  m/s), when the layer thickness is increased to 7 or 8 m or greater.
  - For constant  $k \approx 10^{-4}$  m/s and  $\sigma'_{v0} = 12$  atm,  $K_{dr} \approx 1.45$  if H = 5–10 m, with the factor increasing to  $K_{dr} \approx 1.8$  if the layer thickness decreases to H = 2 m.
- 4. These results of the parametric study provide considerable insight on the combinations of parameters for which the current state-of-practice of using undrained  $K_{\sigma} < 1.0$  becomes too conservative, and should be supplemented with consideration of partial drainage through the use of factor  $K_{\rm dr}$ . It also provides the charts needed to evaluate the value of  $K_{\rm dr}$  in practical applications for a sand layer having a relative density of 45% and free drainage at the top.

The conclusions presented herein correspond to specific soil and drainage conditions which may or may not be applicable if the conditions are changed. Additional centrifuge tests and simulations using the numerical methodology utilized in this paper, are recommended for further evaluation of  $K_{\rm dr}$  and  $(K_{\sigma})_{\rm field}$ , with the numerical studies covering sand relative densities other than 45%, as well as a range of loading cycles, soil profiles and drainage conditions beyond the uniform single sand layer with free top drainage studied in this paper.

#### **Data Availability Statement**

Some or all data, models, or code that support the findings of this study are available from the corresponding author upon reasonable request.

#### Acknowledgments

This research was performed using the FLAC3D demo version provided by Itasca Consulting Group Inc. The authors would like to thank Dr. Zhao Cheng from FLAC3D support team for his guidance during the course of this research. The research was supported by the National Science Foundation under Grants No. 1545026 and 1904313 and NYU Abu Dhabi; this support is gratefully acknowledged.

#### **Supplemental Materials**

Tables S1–S6 are available online in the ASCE Library (www ascelibrary.org).

#### References

- Abdoun, T., M. Ni, R. Dobry, K. Zehtab, A. Marr, and W. El-Sekelly. 2020. "Pore pressure and  $K_{\sigma}$  evaluation at high overburden pressure under field drainage conditions. II: Additional interpretation." *J. Geotech. Geoenviron. Eng.* 146 (9): 04020089. https://doi.org/10.1061/(ASCE)GT.1943-5606.0002302.
- Biot, M. A. 1955. "Theory of elasticity and consolidation for a porous anisotropic solid." J. Appl. Phys. 26 (2): 182–185. https://doi.org/10 .1063/1.1721956.
- Boulanger, R. W. 2003. "High overburden stress effects in liquefaction analyses." J. Geotech. Geoenviron. Eng. 129 (12): 1071–1082. https:// doi.org/10.1061/(ASCE)1090-0241(2003)129:12(1071).
- Boulanger, R. W., and I. M. Idriss. 2004. "State normalization of penetration resistance and the effect of overburden stress on liquefaction resistance." In *Proc.*, 11th SDEE and 3rd ICEGE. Berkeley, CA: Univ. of California.
- Dobry, R., and T. Abdoun. 2015 "Cyclic shear strain needed for liquefaction triggering and assessment of overburden pressure factor K<sub>σ</sub>." J. Geotech. Geoenviron. Eng. 141 (11): 04015047. https://doi.org/10.1061/(ASCE)GT.1943-5606.0001342.
- Elgamal, A. W., M. Zeghal, H. T. Tang, and J. C. Stepp. 1995. "Lotung downhole array. I: Evaluation of site dynamic properties." *J. Geotech. Geoenviron. Eng.* 121 (4): 350–362. https://doi.org/10.1061/(ASCE) 0733-9410(1995)121:4(350).
- El Ghoraiby, M. A., H. Park, and M. T. Manzari. 2017. *LEAP 2017: Soil characterization and element tests for Ottawa F65 sand*. Washington, DC: The George Washington Univ.
- El-Sekelly, W., R. Dobry, and T. Abdoun. 2023a. "Assessment of state-of-practice use of field liquefaction charts at low and high overburden using centrifuge experiments." *Eng. Geol.* 312 (Aug): 106952.
- El-Sekelly, W., R. Dobry, and T. Abdoun. 2023b. "A numerical approach for simulation of stress-controlled cyclic shear loading in a soil column considering partial drainage." Soil Dyn. Earthquake Eng. 174 (Feb): 108191.

- El-Sekelly, W., R. Dobry, T. Abdoun, and M. Ni. 2022. "Evaluation of field sand liquefaction including partial drainage under low and high overburden using a generalized bounding surface model." Soil Dyn. Earthquake Eng. 152 (Jun): 107059. https://doi.org/10.1016/j.soildyn.2021 107059
- Gillette, D. 2013. "Liquefaction issues for dam safety—Bureau of Reclamation." In Proc., Presentation in One-Day Workshop, Committee on State of the Art and Practice in Earthquake Induced Soil Liquefaction Assessment. Washington, DC: National Research Council of the National Academies.
- Hynes, M. E., R. S. Olsen, and D. E. Yule. 1999. "Influence of confining stress on liquefaction resistance." In *Proc., Int. Workshop on Physics* and *Mechanics of Soil Liquefaction*, 145–152. Rotterdam, Netherlands: A.A. Balkema.
- Idriss, I. M., and R. W. Boulanger. 2006. "Semi-empirical procedures for evaluating liquefaction potential during earthquakes." Soil Dyn. Earthquake Eng. 26 (2–4): 115–130. https://doi.org/10.1016/j.soildyn.2004 11.023
- Idriss, I. M., and R. W. Boulanger. 2008. Soil liquefaction during earth-quakes: Monograph MNO-12. Berkeley, CA: Earthquake Engineering Research Institute.
- Manzari, M. T., et al. 2018. "Liquefaction experiment and analysis projects (LEAP): Summary of observations from the planning phase." Soil Dyn. Earthquake Eng. 113 (Oct): 714–743. https://doi.org/10.1016/j.soildyn.2017.05.015.
- Montgomery, J., R. W. Boulanger, and L. F. Harder Jr. 2012. *Examination of the K\sigma overburden correction factor on liquefaction resistance*. Rep. No. UCD/CGM-12-02. Davis, CA: Univ. of California.
- National Academies. 2017. "State of the art and practice in the assessment of earthquake-induced soil liquefaction and its consequences." In A report of the national academies, committee on state of the art and practice in earthquake-induced soil liquefaction. Washington, DC: National Academies Press.
- Ni, M., T. Abdoun, R. Dobry, K. Zehtab, A. Marr, and W. El-Sekelly. 2020. "Pore pressure and  $K_{\sigma}$  evaluation at high overburden pressure under field drainage conditions. I: Centrifuge experiments." *J. Geotech. Geoenviron. Eng.* 146 (9): 04020088. https://doi.org/10.1061/(ASCE)GT .1943-5606.0002303.
- Seed, H. B. 1983. "Earthquake-resistant design of earth dams." In Proc., Seismic Design of Earth Dams and Caverns. Reston, VA: ASCE.
- Seed, H. B., and I. M. Idriss. 1971. "Simplified procedure for evaluating soil liquefaction potential." *J. Soil Mech. Found. Div.* 97 (9): 1249– 1273. https://doi.org/10.1061/JSFEAQ.0001662.
- Seed, R. B., and L. F. Harder Jr. 1990. "SPT-based analysis of cyclic pore pressure generation and undrained residual strength." In *Proc.*, H. Bolton Seed Memorial Symp. Berkeley, CA: Univ. of California.
- Terzaghi, K., R. B. Peck, and G. Mesri. 1996. Soil mechanics in engineering practice. 3rd ed. New York: Wiley.
- Vaid, Y. P., and J. Thomas. 1995. "Liquefaction and postliquefaction behavior of sand." J. Geotech. Eng. 121 (2): 163–173. https://doi.org/10.1061/(ASCE)0733-9410(1995)121:2(163).
- Youd, T. L., and I. M. Idriss. 2001. "Liquefaction resistance of soils: Summary report from the 1996 NCEER and 1998 NCEER/NSF workshops on evaluation of liquefaction resistance of soils." *J. Geotech. Geoenviron. Eng.* 127 (4): 297–313. https://doi.org/10.1061/(ASCE) 1090-0241(2001)127:4(297).
- Zeghal, M., A. W. Elgamal, H. T. Tang, and J. C. Stepp. 1995. "Lotung downhole seismic array: Evaluation of soil nonlinear properties." J. Geotech. Eng. 121 (4): 363–378. https://doi.org/10.1061/(ASCE) 0733-9410(1995)121:4(363).